Effects of high pressure on the structural, magnetic, and transport properties of the itinerant 5*f* ferromagnet U_2Fe_3Ge

M. S. Henriques,[1,*] D. I. Gorbunov,[2,3] A. V. Andreev,[2] Z. Arnold,[2] S. Surblé,[4] S. Heathman,[4] J.-C. Griveau,[4] E. B. Lopes,[1] J. Prchal,[3] L. Havela,[3] and A. P. Gonçalves[1]

[1]*Center of Nuclear Science and Technology - C2TN, IST/CFMCUL, University of Lisbon, Nuclear and Technological Campus, P-2695-066 Bobadela, Portugal*

[2]*Institute of Physics, Academy of Sciences of the Czech Republic, Na Slovance 2, 182 21 Prague, Czech Republic*

[3]*Charles University, Faculty of Mathematics and Physics, Department of Condensed Matter Physics, Ke Karlovu 5, 121 16 Prague, Czech Republic*

[4]*European Commission, Joint Research Centre, Institute for Transuranium Elements, Postfach 2340, 76125 Karlsruhe, Germany*

(Received 30 October 2013; published 10 February 2014)

Crystal structure, magnetic, and transport properties of the U_2Fe_3Ge compound have been studied under hydrostatic pressure. U_2Fe_3Ge crystallizes in the hexagonal crystal structure of the Mg_2Cu_3Si type, an ordered variant of the $MgZn_2$ Laves structure (C14). The Laves phase has proven highly stable; the crystal structure is maintained up to 27 GPa, the highest applied pressure. X-ray diffraction data revealed that the *c* direction, where the shortest U-U bonds lie, is softer than the *a* direction. The bulk modulus B_0 is ∼100 GPa. U_2Fe_3Ge is an itinerant ferromagnet with the Curie temperature $T_C = 55$ K and the spontaneous magnetic moment $M_s = 1\mu_B$ per formula unit at ambient pressure. The two parameters decrease rapidly under pressure with the rates $\mathrm{d}(\ln M_s)/\mathrm{d}p = -0.33$ GPa^{-1} and $\mathrm{d}(\ln T_C)/\mathrm{d}p = -0.27$ GPa^{-1}. The extrapolation of T_C and M_s indicates that the magnetic order will be suppressed between 3 and 4 GPa. Electrical resistivity was found to decrease gradually with increasing pressure. The data in the ferromagnetic state points to the opening of a gap in the magnon spectrum at higher pressures. U_2Fe_3Ge is relatively more sensitive to pressure than isostructural UNi_2.

DOI: 10.1103/PhysRevB.89.054407 PACS number(s): 62.50.−p, 75.30.Gw, 75.10.Lp

I. INTRODUCTION

Magnetic properties of uranium intermetallic compounds are to a great extent determined by the partially filled 5*f* electronic shell. Its wide spatial extent results in the hybridization with the outer electronic orbitals of neighboring atoms. The strength of the hybridization depends on the features of the crystal structure, such as interatomic distances, and on the type and coordination number of the nearest-neighbor atoms [1].

A vast diversity of magnetic properties is observed in intermetallic compounds based on U and Fe where the 5*f*-3*d* hybridization occurs. On the one hand, it can lead, besides the direct 5*f*-5*f* overlap, to a substantial delocalization of the 5*f* states, preventing the formation and ordering of uranium magnetic moments. Examples are the compounds UFeAl and UFeGe, exhibiting Pauli paramagnetism (the magnetic moment associated with the 3*d* itinerant electrons vanishes as well) [2,3]. On the other hand, there exist compounds, such as UFe_2, where both sublattices, U and Fe, are magnetic [4–8].

The most convenient way to determine the nature of the 5*f* electrons in uranium-iron intermetallics is to investigate compounds that have an ordered magnetic moment only within the uranium sublattice (see, e.g., [9–11]). Such a study was recently performed on a U_2Fe_3Ge single crystal [12]. The compound crystallizes in the hexagonal Mg_2Cu_3Si-type structure (space group $P6_3/mmc$), an ordered variant of the $MgZn_2$ Laves structure (C14). The unit cell is shown in Fig. 1, where the U, Fe, and Ge atoms occupy the crystallographic sites 4*f*, 6*h*, and 2*a*, respectively. U_2Fe_3Ge is an unusual system from the viewpoint of magnetism. Despite the short U-U spacing, $d_{U\text{-}U} \leqslant 3.2$ Å, i.e., far below the Hill limit of 3.4 Å for U [13], U_2Fe_3Ge is a ferromagnet below $T_C = 55$ K, and its magnetism is based on the uranium sublattice only. No magnetic splitting was detected by ^{57}Fe Mössbauer spectroscopy down to $T = 4$ K. The short U-U interatomic distances leading to ordered $\mu = 0.5\mu_B$/U and effective $\mu_{eff} = 2.52\mu_B$/U magnetic moments, reduced in comparison with the $5f^2$ and $5f^3$ configurations of U, provide a clear evidence for the itinerant nature of magnetism in U_2Fe_3Ge. The magnetic moments lie in the basal plane of the compound. Within the basal plane, no anisotropy was detected. The type of anisotropy corresponds to a two-ion hybridization-induced anisotropy, but it was found to be relatively weak, the anisotropy field with respect to the *c*-axis orientation being $\mu_0 H_a = 8$ T at $T = 2$ K, whereas typical values for uranium intermetallics are of the order of 10^2 T.

The itinerant nature of the magnetism in U_2Fe_3Ge may render the compound sensitive to variations of the external pressure, since the width, position, and hybridization of the 5*f* band are susceptible to interatomic distances and volume changes. The broadening of the 5*f* band due to reduced interatomic distances leads in typical cases to a reduction of the density of electronic states near the Fermi level, and magnetic moments and ordering temperatures are reduced. Previous high-pressure studies on the isostructural itinerant ferromagnet UNi_2 demonstrated large negative pressure effects on the spontaneous magnetization and the magnetic ordering temperature (see Ref. [14] and references therein). A qualitatively different response to pressure has been observed for U compounds with more localized 5*f* states. The initial increase of the ordering temperature can be understood as due to the strengthening of 5*f*-ligand hybridization, which mediates the exchange interactions [15].

*Corresponding author: mish@ctn.ist.utl.pt

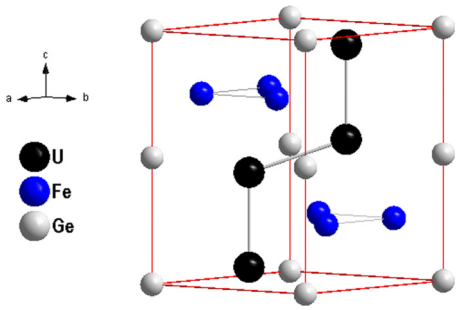

FIG. 1. (Color online) Unit cell of the compound U_2Fe_3Ge.

Although hydrostatic pressure is a convenient technical variable to probe the magnetism, its tuning naturally arises from the lattice compression [16–18]. As the lattice reaction to pressure is different for materials with different bulk moduli (and it can be nonlinear as a function of pressure), the pressure variations of magnetic properties should be complemented by the knowledge of the crystal lattice response and stability under such pressures. In addition, the bulk modulus value can be used as an indicator of the degree of delocalization of the $5f$ states, as shown by high-pressure measurements performed on several binary C15 Laves phases [19].

The situation is further complicated by the elastic anisotropy, which tends to reflect the U-U bonding anisotropy. In general, the direction of the shortest U-U links was found to be the most compressible in the crystal lattice for U compounds, while the U moments tend to orient perpendicular to it [20], in agreement with the theoretical work by Cooper *et al.* [21]. Due to the critical importance of the $5f$-$5f$ overlap, the soft lattice direction in compression seems to be the most direct parameter tuning the magnetic properties, rather than the overall volume.

The goal of the present paper is to establish the connection between structural and electronic properties of U_2Fe_3Ge, studied in single-crystal form under high pressures. X-ray diffraction experiments were performed in order to probe the stability of the crystal structure and to determine the isothermal bulk modulus. The pressure response of electronic properties was studied by magnetization and electrical resistivity measurements.

II. EXPERIMENTAL DETAILS

A single crystal of U_2Fe_3Ge was grown by a modified Czochralski method from a stoichiometric mixture of the pure elements (99.9% U, 99.98% Fe, and 99.99% Ge) on a water-cooled copper crucible in a triarc furnace. A tungsten rod was used as a seed, and the pulling speed was varied between 10 and 30 mm/h. The crystal structure was determined on a part of the single crystal crushed into a fine powder. In order to check the monocrystalline state and to orient the crystal, backscattered Laue diffraction was used.

A small piece of the single crystal was crushed, and the microsample was loaded into a Le Toulec-type diamond anvil cell using a preindented Inconel gasket with a 200-μm-diameter hole. Silicone oil was used as the pressure-transmitting medium, and a ruby chip was added as a pressure gauge via the ruby shift of the laser fluorescence, which follows an argon laser excitation [22].

High-pressure x-ray diffraction was performed at room temperature up to 27 GPa by using a modified Bruker diffractometer with focusing mirror optics installed on a molybdenum rotating anode source (λ (Mo K_a) = 0.70926 Å) coupled with a Bruker Smart Apex II detector system. The recorded diffraction images were integrated using the European Synchrotron Radiation Facility Fit2D software [23]. The FullProf program [24] was used to refine the data by the Le Bail method. The first x-ray diffraction pattern taken at ambient conditions was used as a reference and to check the diffraction angle. The x-ray patterns collected at each pressure p were refined to access the corresponding lattice parameters, $a(p)$ and $c(p)$, and the unit cell volume $V(p)$. The cell parameters were fitted in the low-pressure region to obtain the isothermal linear compressibility and the isothermal bulk modulus B_0. The relative volumes, calculated using $V(p)$ and the initial volume of the hexagonal cell extrapolated to zero pressure (V_0), were adjusted by a first-order Birch-Murnaghan equation of state [25,26]

$$p = \frac{B_0}{B_0'}\left[\left(\frac{V_0}{V(p)}\right)^{B_0'} - 1\right], \tag{1}$$

where B_0' is the pressure derivative of B_0.

The magnetization measurements under hydrostatic pressure up to $p = 0.74$ GPa in the range $T = 5$–100 K were performed in a standard superconducting quantum interference device magnetometer (Quantum Design) in static magnetic fields up to 7 T using a miniature CuBe pressure cell with a liquid pressure-transmitting medium [27]. The values of pressure were determined at low temperatures using the known pressure dependence of the critical temperature of the superconducting state of a Pb sensor placed inside the cell [28]. This method of monitoring pressure has proven to be rather robust at low temperatures, as the pressure drifts with temperature mostly due to different thermal expansion of all parts of the experimental setup (pressure cell, sample, and pressure-transmitting medium). Due to generally low thermal expansion at low temperatures, only a small deviation of pressure is expected below ~100 K.

The high-pressure resistivity measurements were performed on a part of the single crystal up to the maximum pressure of 3.51 GPa. The sample was polished carefully to reach a thickness near 20 μm and loaded with a thin foil of lead into a clamped high-pressure cell. The pressure cell is made of nonmagnetic CuBe and contains two tungsten carbide anvils, a pyrophyllite gasket, and steatite discs as the solid pressure-transmitting medium. The dc resistance is measured using a standard four-probe technique with Pt wires. The temperature is determined by a Cernox thermometer for the whole temperature range (1.5–300 K). At each step, pressure is increased at room temperature and then determined at low temperature using the Pb superconducting transition temperature [28]. For each pressure, a complete T dependence of resistivity was measured down to $T = 1.5$ K using a ^{4}He pumped cryostat.

III. RESULTS AND DISCUSSION

A. High-pressure x-ray diffraction

The structural behavior of U_2Fe_3Ge was studied by x-ray diffraction up to 27 GPa. The lattice parameters at room temperature and ambient pressure for a powdered sample were determined to be $a = 5.186$ Å and $c = 7.852$ Å, which is in good agreement with the data published previously [12]. The x-ray diffraction on the unloaded sample mounted in the pressure cell gave the lattice parameters $a = 5.140$ Å and $c = 7.786$ Å. These lattice parameters differ from those obtained on a conventional powder diffractometer, probably due to misadjustment of the sample position during the experiment. Nevertheless, these values are not critical for the determination of the sample compressibility, and all the resulting calculations were done on the basis of the pressure cell lattice parameters extrapolated to zero pressure, as explained in the previous section.

The patterns collected when increasing the applied pressure were all consistent with the hexagonal Mg_2Cu_3Si structure type, an ordered variant of the binary C14 Laves phase (space group $P6_3/mmc$), as shown in Fig. 2. The U_2Fe_3Ge compound has a close-packed crystal structure, and there is no obvious sign of any structural transition in the pressure range studied, in agreement with the high stability of the Laves phase structure. The clearest observable effect is the peak broadening for high pressures, which corresponds mainly to an imperfect hydrostaticity with increasing applied pressure, as can be better seen in Fig. 3, although more careful studies would be desirable for $p > 10$ GPa in a different pressure-transmitting medium.

A refinement of the high-pressure x-ray diffraction data has been attempted by the Rietveld and Le Bail methods. For the Rietveld refinements, a preferred orientation of U_2Fe_3Ge along the (001) direction, negative Debye-Waller factors for U and Fe atoms, and the presence of reflections from the gasket have shown that many *in situ* experimental effects are difficult to include in the complete structural model. Consequently, the present paper has been restricted to the Le Bail fitting

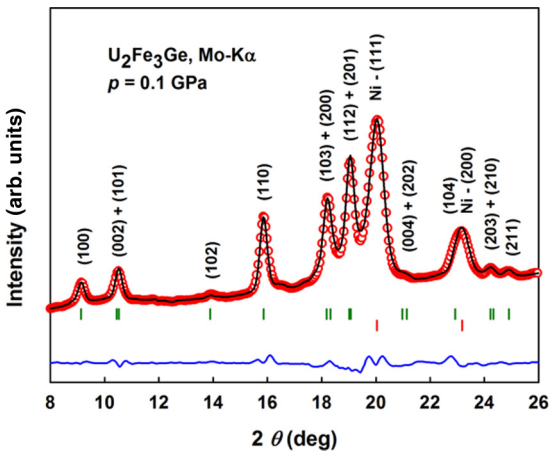

FIG. 2. (Color online) X-ray diffraction pattern of U_2Fe_3Ge taken at 0.1 GPa (red open symbols) with the Le Bail fitting (black line) and the difference profile (bottom blue line). It shows the calculated Bragg positions of U_2Fe_3Ge (green vertical bars) and of the Inconel gasket (red vertical bars), together with the Miller indexes for both.

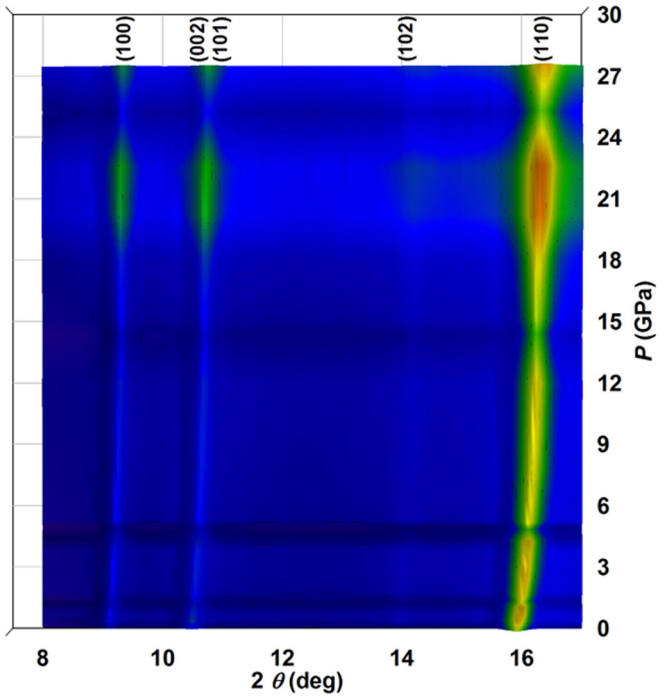

FIG. 3. (Color online) Partial representation of the diffraction patterns taken at different pressures, reflecting the shifting and broadening of the diffraction peaks of U_2Fe_3Ge with increasing applied pressure. The broadening is mostly due to imperfect hydrostaticity.

that, despite being a whole-pattern decomposition procedure, is a suitable method to determine the unit cell parameters in high-symmetry lattices [29].

The evolution of the lattice parameters a and c and of the relative volume V/V_0 with pressure for U_2Fe_3Ge is depicted in Fig. 4. The relative changes $\Delta a/a$, $\Delta c/c$, and $\Delta V/V$ are shown together in Fig. 5. For the whole pressure range studied, it can be seen that both unit cell parameters, and thus the relative cell volume, exhibit an approximately similar tendency of decrease but that the compression along the c axis is slightly higher. The solidification of the silicone oil that is known to occur above 6 GPa leads to nonhydrostatic conditions around the sample, and larger error bars may mask the real compressibility behavior in the higher pressure range. For this reason, the quantitative treatment of the data to analyze the lattice compressibility was limited to the pressure range below 6 GPa, while the data at higher pressures demonstrate mainly that there is apparently no indication of any change of the structure type. The limited resolution of the x-ray patterns may mask small lattice distortions, and identical extinction conditions for $P6_3/mmc$ are provided by other space groups.

The linear compressibility along each lattice direction i (k_i) was calculated by the fitting of the pressure data by a quadratic polynomial equation of the form

$$G_i(p) = g_i(0) - k_i g_i(0) p + k_i' g_i(0) p^2. \qquad (2)$$

For U_2Fe_3Ge, the linear compressibility along a is $k_a = 3.0 \times 10^{-3}$ GPa^{-1}, while along c it is $k_c = 3.7 \times 10^{-3}$ GPa^{-1}. Although the anisotropy is not as striking as in various types of ternary equiatomic intermetallics of the general formula UTX [20], the type of anisotropy observed is in agreement with

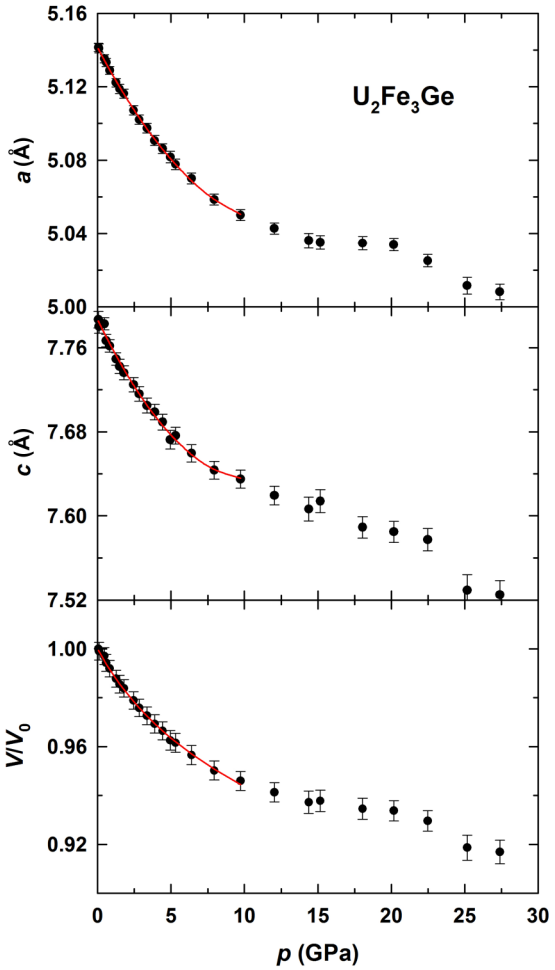

FIG. 4. (Color online) Pressure dependence of the lattice parameters a and c, and relative volume V/V_0 for U_2Fe_3Ge. The full line in the lattice parameters represents the fits according to Eq. (2), while for V/V_0, it corresponds to the fit to the Birch-Murnaghan equation of state according to Eq. (1).

the shortest U-U bonds in U_2Fe_3Ge being along the c direction of the hexagonal unit cell, making it the softest direction in terms of compressibility. The rule that the U moments tend to be perpendicular to the soft lattice direction is thus obeyed. The present results show that this type of anisotropy not only occurs for moderate U-U spacings (as described recently for the UTX compounds and their hydrides [20]) but also remains as a more general trend even for distances as short as 2.75 Å between neighboring U atoms. The questions remain as to whether the relatively weak elastic anisotropy (compared, e.g., with the UTX compounds with the hexagonal ZrNiAl structure type, where a ratio of 1:10 between the compression along the c direction and the basal plane of the lattice is not exceptional [30]) is due to the small inter-U spacing and whether it is related to the relatively weak magnetic anisotropy [12]. However, the U-U interatomic distance depends not only on the lattice parameter c but also on the z coordinate of the U atom in the unit cell. As these variables could not be extracted from the Le Bail analysis performed, the U-U distance cannot be safely claimed to be compressing at the same (or a higher) rate than the unit cell parameter c. Hence, the higher compression along c is not by itself a conclusive proof that the U-U distance is the most compressible in the structure.

The bulk modulus B_0 can be obtained from the pressure-volume data through the relation of the linear compressibilities as $B_0 = 1/k_V$, where k_V is the volume compressibility, which is given by $k_V = 2k_a + k_c$. For U_2Fe_3Ge, these calculations yield $k_V = 0.0097$ GPa^{-1} and $B_0 = 104$ GPa. A different approach to obtain the bulk modulus is to fit the relative volume changes to the Birch-Murnaghan equation of state (Eq. (1)), which resulted in $B_0 = 89$ GPa, in reasonable agreement with the previous calculations. The bulk modulus obtained for isostructural UNi_2, $B_0 = 189$ GPa, and the respective volume compressibility $k_V = 0.005$ GPa^{-1} [19] reveal that U_2Fe_3Ge is considerably softer. The data available for UNi_2 do not allow a full comparison, since we do not know the linear compressibilities and error bars in the measurements performed on this compound. The unit cell of UNi_2 is slightly smaller than that of U_2Fe_3Ge, but the ratio c/a is larger for UNi_2, which is true also for the shortest U-U distances (3.03 Å). The larger c parameter in UNi_2 might be related with a small distortion (<1%) in the Ni sublattice (when compared with an ideal Laves phase), whereas for the Fe-Ge sublattice in U_2Fe_3Ge, it is close to 5%. This might be one of the contributions to the lower bulk modulus of U_2Fe_3Ge in comparison with UNi_2, although one should be aware of other contributions that may play essential roles (as the magnetic anisotropy), as will be further discussed in this paper.

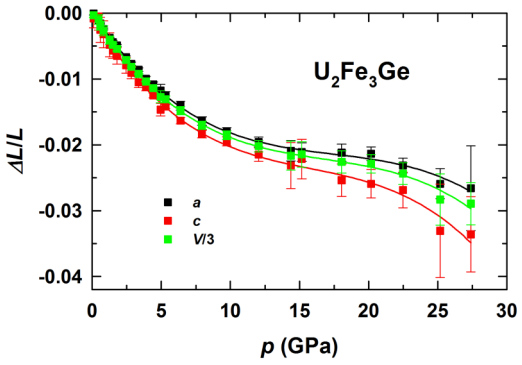

FIG. 5. (Color online) Pressure changes of the relative lattice parameters $\Delta a/a$ and $\Delta c/c$ and volume $\Delta V/V$ for U_2Fe_3Ge.

B. Magnetization

The temperature dependence of the magnetization at various pressures measured along the easy a axis of the U_2Fe_3Ge single crystal is shown in Fig. 6. All $M(T)$ curves display characteristic ferromagnetic type of behavior. The phase transition into the paramagnetic state can be associated with the rapid drop of the magnetization in the vicinity of $T = 50$ K on the curves measured in a low field of 0.01 T. Figure 6 clearly indicates a shift of the Curie temperature to lower temperatures with increasing pressure. The data taken in a field of 2 T exhibit the transition naturally smeared out but allow us to assess the pressure variations of magnetic moment, which also exhibits a decreasing tendency.

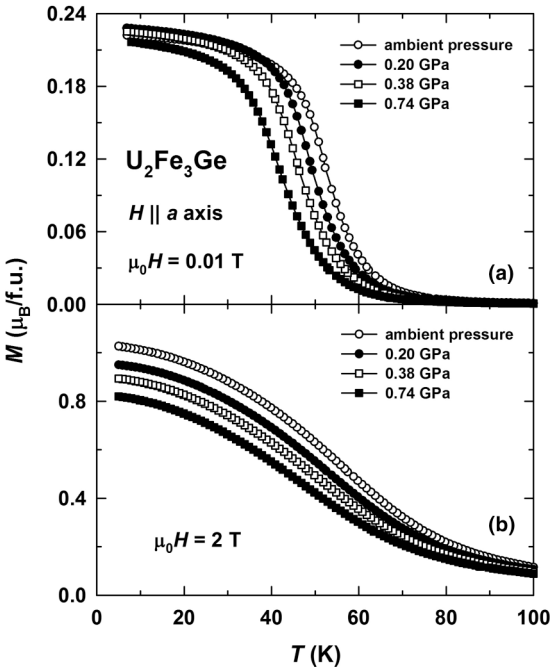

FIG. 6. Temperature dependence of the magnetization along the a axis of the U_2Fe_3Ge single crystal in a field of (a) 0.01 T and (b) 2 T under different pressures. Note the different magnetization scales in the two panels.

Figure 7 demonstrates the effect of pressure on magnetization curves along the a axis of the U_2Fe_3Ge single crystal at $T = 2$ and 50 K. The application of pressure results in a decrease of the magnetization. The spontaneous magnetic

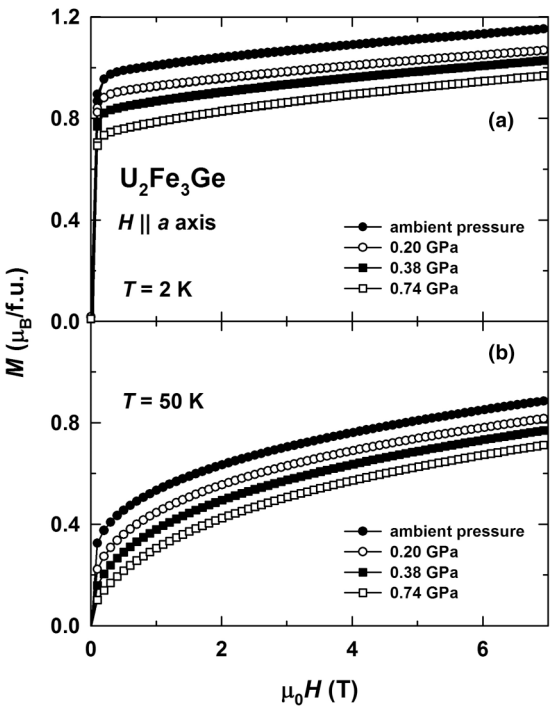

FIG. 7. Magnetization curves along the a axis of the U_2Fe_3Ge single crystal at (a) $T = 2$ K and (b) $T = 50$ K at various pressures.

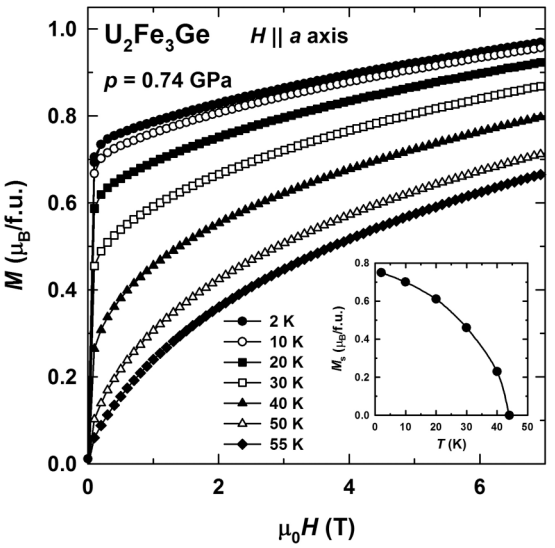

FIG. 8. Temperature evolution of the magnetization curve along the a axis of the U_2Fe_3Ge single crystal under $p = 0.74$ GPa. The inset shows the temperature dependence of the spontaneous magnetic moment under this pressure.

moment determined from the corresponding Arrott plot is about $M_s = 1.0\mu_B$ per formula unit (f.u.) at $T = 2$ K at ambient pressure, which agrees with previous data obtained without the pressure cell [12]. A monotonous reduction of the M_s value down to $0.75\mu_B$/f.u. at $p = 0.74$ GPa can be deduced. The high-field differential susceptibility dM/dH remains approximately the same even under pressure.

The temperature $T = 50$ K was chosen to give the ordered state (seen as the presence of a spontaneous moment) at ambient pressure (and at $p = 0.2$ GPa), but the pressure-induced shift of T_C leads to the paramagnetic state (no spontaneous moment) at elevated pressures at this temperature.

Figure 8 shows the temperature evolution of the magnetization curve along the a axis of the U_2Fe_3Ge single crystal for the highest pressure $p = 0.74$ GPa. The $M(H)$ curves are qualitatively similar to those at ambient pressure (see Fig. 7 of Ref. [12]). A nonzero spontaneous magnetic moment is observed at $T = 40$ K but disappears when approaching $T = 50$ K. The temperature dependence of the spontaneous magnetic moment is shown in the inset in Fig. 8.

The results of the magnetic study of U_2Fe_3Ge under pressure are summarized in Fig. 9(a), which shows the pressure dependence of the spontaneous magnetic moment at $T = 2$ K and of the Curie temperature. Both parameters display a practically linear decrease with pressure. They are sensitive to the external pressure, which is manifested by rather high relative decrease rates, $d(\ln M_s)/dp = -0.33$ GPa^{-1} and $d(\ln T_C)/dp = -0.27$ GPa^{-1}. A tentative linear extrapolation of the $T_C(p)$ dependence to zero shows that the magnetic order in U_2Fe_3Ge will be suppressed in the pressure range 3–4 GPa. The linear fits give $T_C(p) = 0$ at $p = 3.7$ GPa, while $M_s(p) = 0$ at $p = 3.0$ GPa. Plotting M_s and T_C as a function of the relative change in the c parameter in compression gives a somewhat better linearity of the respective data points. We obtained $T_C(V/V_0) = 0$ at $V/V_0 = 0.963$ and $M_s(V/V_0) = 0$ at $V/V_0 = 0.970$. Such values yield approximately the same

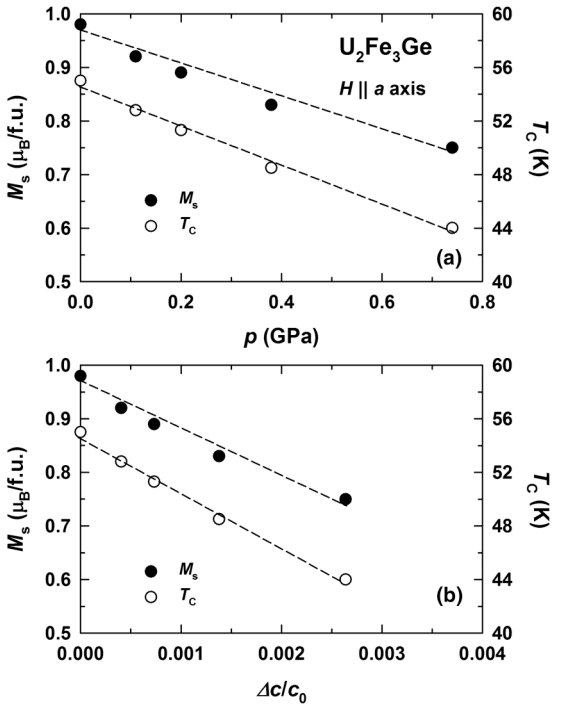

FIG. 9. (a) U_2Fe_3Ge spontaneous magnetic moment and Curie temperature dependence as a function of pressure, and (b) relative change of the c parameter.

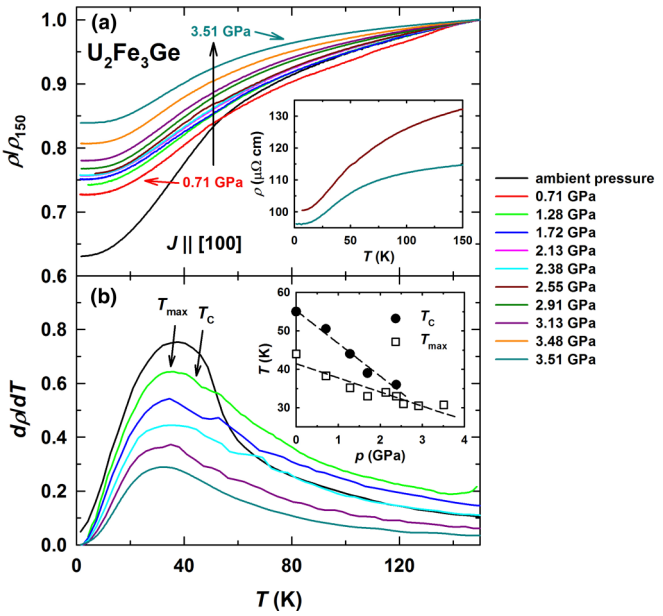

FIG. 10. (Color online) (a) Temperature dependence of the normalized electrical resistivity ρ, and (b) several temperature derivatives for pressures in the range $p = 0.71$–3.51 GPa for U_2Fe_3Ge with current flowing along the a axis. The inset in panel (a) presents the electrical resistivity in absolute values at $p = 2.55$ GPa (bottom) and 3.51 GPa (top). The temperature derivatives showing the evolution of T_C and T_{max} with the pressure are plotted in the inset of panel (b). The arrows on the $d\rho/dT(T)$ dependence show the position of T_C and T_{max}.

critical pressures as those given above. The magnetic order should be lost at $V = 171$ Å^3, which corresponds to $c = 7.682$ Å, as deduced from the linear extrapolation of T_C and M_s as a function of the c-axis compression (Fig. 9(b)).

C. Electrical resistivity

Figure 10(a) presents the temperature dependence of the electrical resistivity of U_2Fe_3Ge taken at various applied pressures, using the current flowing along the a axis. The resistivity at ambient conditions is $\rho_{295K} = 139$ $\mu\Omega$cm, and a distinct change in the slope coincides with the onset of the ferromagnetic transition.

The low-temperature $\rho(T)$ data (1.5–15 K) can be tentatively described as

$$\rho = \rho_0 + AT^2, \tag{3}$$

where ρ_0 is the residual resistivity due to impurities and defects ($\rho_0 = 93$ $\mu\Omega$cm at ambient pressure) and A is a parameter dependent on the density of the electronic states at the Fermi energy, which influences the electron-electron scattering ($A = 29 \times 10^{-3}$ $\mu\Omega$cm K^{-2}). These values are similar to the results obtained for U_2Fe_3Ge polycrystals [31]. The A coefficient is related to the Sommerfeld coefficient γ of the electronic specific heat by the empirical Kadowaki-Woods relation $A/\gamma^2 \approx 10^{-5}$ $\mu\Omega$cm mJ^{-2} K^2 mol^2 [32]. Although this relation is in principle valid mostly for highly correlated, nonmagnetically ordered systems, the experimental A value obtained through it gives a Sommerfeld coefficient $\gamma \approx 54$ mJ mol^{-1} K^{-2} for U_2Fe_3Ge, which is in reasonable agreement with the experimental value $\gamma = 44$ mJ mol$_U^{-1}$ K^{-2} [12]. The reason might be that there is a possibly different value of A for current along c (which has not been studied) or that there is an additional contribution to resistivity due to the spin-disorder scattering. We cannot identify it for ambient pressure data, but it becomes visible at elevated pressures.

The measurements under pressure, performed on a smaller sample with similar orientation, were normalized at $T = 150$ K. The necessity of normalization comes from the ability of the contacts to shift somewhat between successive pressure steps. This frequently happens, especially in the low-pressure range due to induced changes in the form factors. Therefore, the overall flattening, evident with increasing pressure in Fig. 10, can be in general due to either increasing the residual resistivity or decreasing the resistivity at higher temperatures. The first reason seems to be less plausible, as the residual resistivity is affected mainly by structural defects (although it can depend on the density of states at E_F, providing final states for individual scattering events, or, e.g., on magnetic moments of antistructure atoms). The reduction of the spin-disorder scattering by suppressing the size of moments is a more likely reason, leading to the decrease of high-temperature resistivity. The absolute values of resistivity at 300 K tend to decrease (by ~5%) from $p = 2.55$–3.51 GPa, while ρ_0 values exhibit a weakly increasing tendency (Fig. 10(a), inset).

A tentative analysis of the data in the low-T limit reveals that the quadratic power law becomes less satisfactory at elevated pressures. As spin-wave excitations are possible in ferromagnets with weak anisotropy, we attempted to use the

formula

$$\rho = \rho_0 + AT^2 \exp(-\Delta/T), \quad (4)$$

where the second term describes the scattering of the conduction electrons on spin-wave excitations with a gap Δ in the spin-wave spectrum. The energy gap obtained is 1 K (0.086 meV) at 0.71 GPa and grows to 20 K (1.7 meV) at 3.51 GPa. Such a type of analysis might not be necessarily significant, because both the quadratic and the exponential terms should be present simultaneously. Too many fitting parameters, however, make the analysis rather arbitrary in this case.

The Curie temperature cannot be distinguished well directly from the $\rho(T)$ data. Figure 10(b) reveals that it can be associated with an anomaly seen in the first temperature derivative $d\rho/dT$. But as T_C shifts to lower temperatures with pressure, it merges with the maximum resistivity slope and we lose the resolution. The inset Fig. 10(b) shows this negative pressure effect on T_{max} (the temperature where the slope is maximal) and in the Curie temperature itself. The pressure dependence of the Curie temperature shows a trend in the resistivity measurements similar to the one found in the magnetization measurements in the previous section. Moreover, the T_C values obtained from the magnetization and resistivity measurements are in good agreement, with the critical pressure estimated to be above 3 GPa.

IV. DISCUSSION AND CONCLUSIONS

The present paper on the systematic study of U_2Fe_3Ge aimed to relate the evolution of its crystal structural and electronic properties under high pressure. Such a study helps to clarify the role of the $5f$ states in the magnetic and transport properties of the compound. The hexagonal crystal structure of U_2Fe_3Ge was shown to be stable up to the highest available pressure. The linear compressibility of U_2Fe_3Ge was found to be anisotropic, being 23% higher along the c axis in comparison with the a axis. The $5f$ charge density is in many cases compressed to the direction of the shortest U-U links. The sensitivity of the $5f$ states to external variables, such as pressure, causes this direction to be the softer direction of the structure. Our findings on U_2Fe_3Ge are consistent, which indicates that the concept of directional $5f$ bonding is valid even for very small U-U spacings, yet they lead to a paradox: the closer together the U atoms are in a certain direction, the easier they still can be pressed together by external pressure.

The pressures applied in the magnetization experiment indicate a rapid reduction of both ordered moments and critical temperatures. The pressure needed to suppress ferromagnetism entirely can be roughly estimated as 3–4 GPa.

Large pressure effects on the spontaneous magnetization in the zero temperature limit and on the Curie temperature can be expected in systems with low temperatures of magnetic ordering and/or low magnetic moments. For such systems, the relative pressure dependence of these parameters is negative and on the same order of magnitude, which can be understood in the frame of the Stoner-Wohlfarth model for weak itinerant ferromagnetism [33]. In the case of U_2Fe_3Ge, the pressure derivatives found in the present paper ($d(\ln M_s)/dp = -0.33$ GPa^{-1} and $d(\ln T_C)/dp = -0.27$ GPa^{-1}) are both

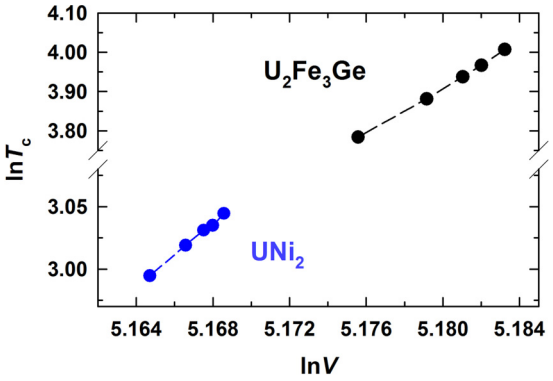

FIG. 11. (Color online) Derivative of the logarithmic dependence of T_C against the volume plotted for U_2Fe_3Ge and UNi_2, showing how the same range of pressure affects both compounds. The dashed lines are guides to the eye.

negative and close in absolute value, bringing further evidence of the itinerant magnetism of this compound. For UNi_2, a system similar to U_2Fe_3Ge from the viewpoints of the crystal lattice and of the U-based itinerant magnetism, it was found that $d(\ln M_s)/dp = -0.1$ GPa^{-1} and $d(\ln T_C)/dp = -0.067$ GPa^{-1} [34]. From these pressure derivatives, one can see immediately that the magnetic order in U_2Fe_3Ge is more sensitive to pressure than in UNi_2, although the values are comparable for the two materials. The critical pressure to suppress ferromagnetism was estimated to be 3–4 and 30 GPa for U_2Fe_3Ge and UNi_2 [34], respectively. To make it clear, a graphical comparison is made between the ln T_C and the ln V function for UNi_2 and U_2Fe_3Ge for the same pressure range (Fig. 11). It illustrates how much smaller these changes are for UNi_2 when compared with U_2Fe_3Ge. This has to be related to U_2Fe_3Ge being more compressible (the isothermal compressibility $(1/V)(dV/dp)$ is $d(\ln V)/dp$). The logarithmic volume derivative $d(\ln T_C)/d(\ln V)$ is 29 for U_2Fe_3Ge and 13 for UNi_2, stressing the difference between the two compounds observed in the present paper. This is somewhat surprising, as UNi_2 has much lower T_C (<30 K) and μ_s (<0.1μ_B/f.u.) [14].

In a single-crystal study, it was found that the magnetic moments of U_2Fe_3Ge lie in the basal plane of the hexagonal lattice, and no anisotropy was detected within the basal plane (magnetization along the [100] and [120] axes showed identical behavior) at ambient conditions [12]. The appearance of a gap in the magnon spectrum under pressure would reflect that the crystal lattice lowers the symmetry and that magnetic anisotropy is induced within the basal plane of the compound. That is, the gap denotes the energy difference between nonequivalent axes within the basal plane.

The possible increase in the anisotropy of U_2Fe_3Ge with pressure is highly unusual, since band broadening should lead to a more isotropic character of hybridization. However, it may happen if, for instance, intrinsic and magnetoelastic contributions to the anisotropy are mutually canceled, similar to the case of UFe_2 [35]. Increasing pressure in this case may shift the balance between them, leading to an overall increase in the anisotropy. In order to confirm or disprove this assumption, magnetostriction measurements should be performed on a U_2Fe_3Ge single crystal.

It would also be interesting to perform magnetization measurements under pressure at which the gap evolves in order to observe the induced anisotropy of magnetization within the basal plane directly. Unfortunately, the experimental setup used in the present paper does not allow us to do this. Nevertheless, the gap is very narrow, and consequently, the anisotropy within the basal plane is weak, even at the highest available pressure. Precise measurements are required to detect the in-plane anisotropy of magnetization.

The situation at the Fermi level has to affect the electrical resistivity. At ambient conditions, U_2Fe_3Ge and UNi_2 have a similar density of states at the Fermi level, according to the comparable Sommerfeld coefficients obtained from the specific heat measurements ($\gamma = 44$ mol$_U^{-1}$ K^{-2} for U_2Fe_3Ge and $\gamma = 65$ mJ mol^{-1} K^{-2} for UNi_2) [12,36]. This parameter does not seem to be further enhanced with pressure, since for U_2Fe_3Ge, the resistivity decreases with increasing pressure. The band broadens, lowering $N(E_F)$, in agreement with reduction of the magnetization and Curie temperature. The spin-disorder resistivity becomes lower, in agreement with the lowering magnitude of magnetic moments with pressure.

In conclusion, in the present work it was determined how the crystal structure, magnetic, and transport properties of the hexagonal Laves phase U_2Fe_3Ge compound evolve under pressure. Although more compressible in comparison with the other representative of the Laves phase compounds, UNi_2, the crystal structure of U_2Fe_3Ge is preserved up to a high pressure. The compressibility was found to be anisotropic. The softer direction is the c axis, where the U-U atoms are at the shortest distances, which reflects the directional $5f$ bonding. The itinerant nature of the $5f$ electrons in ferromagnetic U_2Fe_3Ge is represented by a strong reduction of the Curie temperature, spontaneous magnetic moment, and electrical resistivity under pressure.

ACKNOWLEDGMENTS

The single-crystal growth and part of ambient-pressure magnetization measurements were performed at the Magnetism and Low-Temperature Laboratories supported within the Program of Czech Research Infrastructures (Project No. LM2011025). The work has also been supported by Czech Science Foundation (Grants No. 204/12/0150 and No. P204/10/0330) and by the Portuguese Foundation for Science and Technology–Academy of Sciences of the Czech Republic 2012 bilateral collaboration between Portugal and the Czech Republic. D.I.G. acknowledges Charles University (Grants No. SVV-2013-267303 and No. GAUK-703912). M.S.H. acknowledges the support of the Portuguese Foundation for Science and Technology through the Grant No. SFRH/BD/66161/2009 and the access to infrastructure and support to users provided by the European Commission, Directorate-General, Joint Research Centre, within its "Actinide User Laboratory" program at the Institute for Transuranium Elements, Karlsruhe.

[1] D. D. Koelling, B. D. Dunlap, and G. W. Crabtree, Phys. Rev. B **31**, 4966 (1985).
[2] R. Troć, V. H. Tran, F. G. Vagizov, and H. Drulis, J. Alloys Compd. **200**, 37 (1993).
[3] L. Havela, A. Kolomiets, V. Sechovský, M. Diviš, M. Richter, and A. V. Andreev, J. Magn. Magn. Mater. **177–181**, 47 (1998).
[4] Y. Hamaguchi, N. Kunitomi, S. Komura, and M. Sakamato, J. Phys. Soc. Jpn. **17**, 398 (1962).
[5] M. Yessik, J. Appl. Phys. **40**, 1133 (1969).
[6] L. Paolasini, R. Caciuffo, B. Roessli, G. H. Lander, K. Myers, and P. Canfield, Phys. Rev. B **59**, 6867 (1999).
[7] P. K. Lawson, M. J. Cooper, M. A. G. Dixon, D. N. Timms, E. Zukowski, F. Itoh, and H. Sakurai, Phys. Rev. B **56**, 3239 (1997).
[8] V. N. Antonov, B. N. Harmon, and A. N. Yaresko, Phys. Rev. B **68**, 214424 (2003).
[9] R. Jardin, J.-C. Griveau, K. Prokeš, K. Gofryk, A. V. Kolomiets, P. Normile, S. Heathman, E. Colineau, F. Wastin, and J. Rebizant, Phys. Rev. B **79**, 014409 (2009).
[10] M. Kučera, J. Kuneš, A. Kolomiets, M. Diviš, A. V. Andreev, V. Sechovský, J.-P. Kappler, and A. Rogalev, Phys. Rev. B **66**, 144405 (2002).
[11] N. V. Mushnikov, T. Goto, K. Kamishima, H. Yamada, A. V. Andreev, Y. Shiokawa, A. Iwao, and V. Sechovsky, Phys. Rev. B **59**, 6877 (1999).
[12] M. S. Henriques, D. I. Gorbunov, J. C. Waerenborgh, L. Havela, A. B. Shick, M. Diviš, A. V. Andreev, and A. P. Gonçalves, J. Phys. Condens. Matter **25**, 066010 (2013).
[13] H. H. Hill, in *Plutonium 1970 and Other Actinides*, edited by W. N. Miner (AIME, New York, 1970), p. 2.
[14] J. J. M. Franse, J. Less Common Met. **121**, 73 (1986).
[15] A. Kolomiets, L. Havela, J. Prchal, and A. V. Andreev, J. Korean Phys. Soc. **62**, 1572 (2013).
[16] B. Woo, S. Seo, E. Park, J. H. Kim, D. Jang, T. Park, H. Lee, F. Ronning, J. D. Thompson, V. A. Sidorov, and Y. S. Kwon, Phys. Rev. B **87**, 125121 (2013).
[17] J. Wang, Y. Feng, R. Jaramillo, J. van Wezel, P. C. Canfield, and T. F. Rosenbaum, Phys. Rev. B **86**, 014422 (2012).
[18] G. Quirion, F. S. Razavi, M. L. Plumer, and J. D. Garrett, Phys. Rev. B **57**, 5220 (1998).
[19] S. Dabos, J. S. Olsen, L. Gerward, U. Benedict, and J. C. Spirlet, J. Less Common Met. **142**, L19 (1988).
[20] S. Mašková, A. M. Adamska, L. Havela, N.-T. H. Kim-Ngan, J. Przewoźnik, S. Daniš, K. Kothapalli, A. V. Kolomiets, S. Heathman, H. Nakotte, and H. Bordallo, J. Alloys Compd. **522**, 130 (2012).
[21] B. R. Cooper, R. Siemann, D. Yang, P. Thayamballi, and A. Banerjea, *Handbook on the Physics and Chemistry of the Actinides*, edited by A. J. Freeman and G. H. Lander (Elsevier, Amsterdam, 1985), Vol. 2, p. 435.
[22] H. K. Mao, P. M. Bell, J. W. Shanner, and D. J. Steinberg, J. Appl. Phys. **49**, 3276 (1978).
[23] P. Hammersley, S. O. Svensson, H. Hanfland, A. N. Fitch, and D. Häusermann, High Press. Res. **14**, 235 (1996).

[24] J. Rodríguez-Carvajal, Phys. B **55**, 192 (1993).
[25] F. Birch, Phys. Rev. **71**, 809 (1947).
[26] F. Murnaghan, Am. J. Math. **49**, 235 (1937).
[27] J. Kamarád, Z. Machátová, and Z. Arnold, Rev. Sci. Instrum. **75**, 5022 (2004).
[28] B. Bireckoven and J. Wittig, J. Phys. E Sci. Instrum. **21**, 841 (1988).
[29] V. K. Peterson, Powder Diffr. **20**, 14 (2005).
[30] L. Havela, M. Diviš, V. Sechovský, A. V. Andreev, F. Honda, G. Oomi, Y. Méresse, and S. Heathman, J. Alloys Compd. **322**, 7 (2001).
[31] S. K. Dhar, K. V. Shah, P. Bonville, P. Manfrinetti, and F. Wrubl, Solid State Comm. **147**, 217 (2008).
[32] K. Kadowaki and S. B. Woods, Solid State Comm. **58**, 507 (1986).
[33] J. J. M. Franse, P. H. Frings, A. Menovsky, and A. de Visser, Phys. B **130**, 180 (1985).
[34] J. J. M. Franse, J. Magn. Magn. Mater. **31–34**, 819 (1983).
[35] A. V. Andreev and R. Z. Levitin, J. Alloys Compd. **337**, 18 (2002).
[36] C. Schnitzer, E. Gmelin, and G. Hilscher, Phys. B **130**, 237 (1985).